Materials Transactions, Vol. 52, No. 6 (2011) pp. 1148 to 1155

Abnormal Behavior of Hydrogen Response and Hydrogen Induced Linear Expansion Coefficient of Pd-Cu-Si Metallic Glassy Alloys for Thin Film Hydrogen Sensor

Susumu Kajita[1], Yuki Hasebe[1], Toshiharu Fukunaga[2] and Eiichiro Matsubara[3]

[1]*Advanced Materials Development Department, Panasonic Electric Works Co., Ltd., 1048, Kadoma 571-8686, Japan*
[2]*Research Reactor Institute, Kyoto University, Kumatori-cho, Sennan-gun, Osaka 590-0494, Japan*
[3]*Department of Materials Science and Engineering, Kyoto University, Kyoto 606-8501, Japan*

Thin films of Pd-Cu-Si metallic glassy alloys of varying composition were prepared by simultaneous three sources (Pd, Cu and Si) sputtering method using a rotating mechanism of substrates. Their H_2 responses were observed by measuring the electric resistance changes of them exposed in N_2 and H_2. In addition, their linear expansion coefficients (LECs) induced by absorbed hydrogen were also measured.

Contrary to a normal H_2 response transient with a rapid increase in electric resistance of a thin film, several thin films indicated abnormal H_2 response transients consisting of complex changes, an increase and a decrease, in electric resistance when the thin films were exposed in H_2. These thin films have higher Pd/Si atomic ratios than those indicated normal H_2 response transients. Additionally, by the characterization of the thin films, the existence of Pd-nanocrystals of about 2 nm in diameter was observed in the amorphous matrix which possibly includes Pd-clusters as well as Pd atoms.

The mechanism of the abnormal H_2 response transient can be explained by two conflicting behaviors in electric resistance of the thin films when they are exposed in H_2: a decrease by the formation of electrical contacts of Pd-nanocrystals connected with volume expanded Pd-clusters by hydrogen absorption and a following increase by hydrogenation of Pd-nanocrystals. Observed time lags between two conflicting behaviors can be explained by the different transfer speeds of hydrogen relating to two kinds of pathways: inside of Pd-nanocrystals and the amorphous matrix along which hydrogen atoms transfer in the structure.

The Pd-nanocrystals also affected on LEC and the H_2 response significantly. The thin films with them indicated much higher LEC than the thin films without them. However, the thin films with them did not indicate the high H_2 response expected from their high LEC. The result of LEC suggests that Pd-nanocrystals can absorb much more hydrogen atoms than Pd in an amorphous matrix. The Pd in an amorphous matrix is supposed to be Pd-clusters, randomly distributed Pd atoms and Pd atoms forming a trigonal prism that is a structural unit of the Pd-Cu-Si alloys. On the other hand, the high H_2 response according to the high amount of absorbed hydrogen can not be expected in the thin films with Pd-nanocrystals, due to a decrease in electric resistance by forming electrical contacts of the Pd-nanocrystals.
[doi:10.2320/matertrans.M2010356]

(Received October 13, 2010; Accepted March 8, 2011; Published May 25, 2011)

Keywords: *palladium-copper-silicon alloy, metallic glassy alloy, sputtering, thin film, hydrogen sensor*

1. Introduction

In recent years, research and development relating to hydrogen energy and fuel cells have been conducted all over the world to solve the environmental problems such as drying up of the fossil fuel and global warming caused by excessive CO_2 emission. Above all, development of fuel cell vehicles is now in the limelight, and new types of hydrogen sensor are required for the fuel cell vehicles.[1)]

In order to develop the hydrogen sensor, we adopted a Pd-Cu-Si metallic glassy alloy[2)] that is a typical composition of Pd-based metallic glassy alloys for the sensor material. Palladium has excellent properties as hydrogen sensor material. Pd absorbs about 900 times its volume of hydrogen at room temperature. The electric conductivity of Pd decreases as the amount of hydrogen absorbed in Pd increases.[3)]

According to Lewis,[4)] the electric resistance (R) of a Pd film with hydrogen at room temperature is related to the hydrogen concentration (H/Pd: atomic ratio of absorbed hydrogen to Pd) in the following equation;

$$\mathrm{H/Pd} = 0.9 \times (R - R_0)/R_0$$

where R_0 is the resistance of a Pd film without hydrogen. Baba *et al.*[5)] have studied the variation of electric resistance (R/R_0) with H/Pd for Pd and Pd-Si-based amorphous alloys. In both studies, the electric resistances (R/R_0) of Pd and Pd-Si-based amorphous alloys increase linearly with increasing H/Pd.

In contrast, Pd expands its volume by hydrogen absorption. According to Wicke *et al.*,[6)] absorbed hydrogen atom occupies a part of the octahedral site of fcc-Pd host lattice, resulting in the volume expansion of the Pd-lattice. Salama *et al.*[7)] have reported the volume expansion coefficient (Δ: VEC) of Pd is given by

$$\Delta = (\Delta V/V_0) \times (\mathrm{H/Pd})$$

where V_0 is the atomic volume of Pd and ΔV is the characteristic volume change per H atom. And they indicated $\Delta V/V_0 = 0.19 \pm 0.01$ for the Pd-H system. The linear expansion coefficient is one third of the volume expansion coefficient.

A metallic glassy alloy is a kind of amorphous alloys, and has glass transition temperature (T_g) and wide composition range for forming amorphous phase. A metallic glassy alloy has not grain-boundaries and crystalline defects, resulting in good corrosion resistance and excellent mechanical properties.[8)] It also shows no plateau pressure in pressure composition isotherms using hydrogen gas,[9)] therefore it does not show hysteresis in the change of electric resistance relating to H_2 concentration.

For applying the Pd-Cu-Si metallic glassy alloy to the hydrogen sensor, it must be in a thin film form, because a rapid response to hydrogen is required for the hydrogen

sensor. For example, 90% response must be indicated within 1 s.[1)]

Some investigations of fabricating the metallic glassy alloys in a thin film form have been made to apply the alloys to micro-electro-mechanical systems (MEMS) devices[10)] and sensor devices.[11)] Liu *et al.*[12)] have fabricated thin films of a Pd-Cu-Si metallic glassy alloy by sputtering method with a Pd-Cu-Si alloy target which was prepared by arc-melting mixtures of constituent elements. This method needs to prepare several targets of different compositions for fabricating the thin films in varying composition ratios. Some other sputtering methods that enable convenient control of the composition have been investigated. Yamauchi *et al.*[13)] have fabricated thin films of Pd-Cu-Si metallic glassy alloys of varying composition by combinatorial arc plasma deposition (CAPD) and sputtering method with simultaneous three sources (Pd, Cu and Si) and a rotating mechanism of substrates. Sakurai *et al.*[14)] have fabricated thin films of Cu-Zr metallic glassy alloys of varying composition with a carousel-type sputtering system. They adjusted the RF powers for two kinds of targets (Cu and Zr) individually with rotating substrates to control the composition of the thin films.

In this study, Pd-Cu-Si thin films of varying composition were fabricated by simultaneous three sources (Pd, Cu and Si) sputtering method using a rotating mechanism of substrates. We observed the H_2 responses of them by measuring the electric resistance changes of the thin films exposed in N_2 and H_2. As a result, abnormal H_2 response transients were observed in several thin films. And also, we measured hydrogen induced linear expansion coefficients (LECs) of the thin films, and obtained the characteristic correlation between LEC and Pd/Si atomic ratio. The obtained results of the H_2 response and LEC were discussed from a viewpoint of the microstructures of metallic glassy alloys.

2. Experimental

2.1 Alloy film preparation

The Pd-Cu-Si thin films of varying composition were deposited on glass substrates with an RF magnetron sputtering equipment (L-332FHS, Cannon ANELVA Corporation) having a simultaneous three sources (Pd, Cu and Si) sputtering mechanism and a substrates rotating mechanism. The diameters of sputtering targets (Pd, Cu and Si) were 76.2 mm each. The rotation speed of substrates was fixed at 80 rpm. The substrate-target distance (S-T distance) was 70 mm. Ar-pressure for the sputtering was 0.3 Pa. The composition of thin films was controlled by changing RF power to the three kinds of sputtering targets individually. First of all, we separately measured the each deposition rate of Pd, Cu and Si by changing RF power with rotating substrates at 80 rpm. Figure 1 shows the deposition rates of Pd, Cu and Si against RF power under the sputtering conditions described above. The deposition rate (nm/rev.) is defined as the deposition thickness per one revolution of substrates. In order to fabricate Pd-Cu-Si alloys in amorphous phase, the three elements should be mixed homogeneously in the alloys. If a deposition rate of an element is larger than the corresponding atomic diameter, it leads to the formation of a single element layer in the thin film. In order to obtain a structure of homogeneously mixed elements, a sparse deposition is required. Therefore, the deposition rate of each element should be smaller than the corresponding atomic diameter.

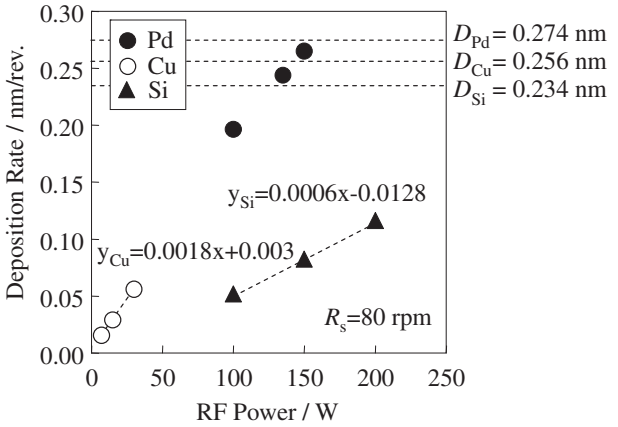

Fig. 1 Deposition rates of Pd, Cu and Si during one revolution of substrates. D_{Pd}: Atomic diameter of Pd D_{Cu}: Atomic diameter of Cu D_{Si}: Atomic diameter of Si R_s: Rotation speeds of substrates y_{Cu}: Deposition rate of Cu by linear approximate equation y_{Si}: Deposition rate of Si by linear approximate equation x: RF Power.

The composition ranges for $Pd_xCu_ySi_z$ amorphous alloys have been reported as follows: $x = 65$–80, $y = 3$–19 and $z = 16$–20.5.[15,16)] Pd content is largest among those of three kinds of elements. Therefore, we fixed the RF power for Pd and controlled those for Cu and Si according to the designed compositions of Pd-Cu-Si alloys. Additionally, the RF power for Pd should be as high as possible, because Cu content is much lower than Pd content in the composition ranges mentioned above, which required much lower RF power for Cu than that for Pd. Of course, the RF power should be within the controllable limit of an equipment. The atomic diameter of Pd (D_{Pd}) is 0.274 nm. We fixed the RF power for Pd to 150 W, at which the deposition rate was 0.265 nm/rev. (see Fig. 1). The RF powers for Cu and Si were calculated using each linear approximate equation relating the deposition rate to the RF power. The equations of Cu and Si are described in Fig. 1. The atomic diameters of Cu (D_{Cu}) and Si (D_{Si}) are 0.256 nm and 0.234 nm, respectively.

The deposition time was calculated to achieve 4000 nm thickness Pd-Cu-Si thin films by using the total deposition rate which is the sum of the deposition rates of three kinds of elements. After measuring the thickness of a deposited thin film, the total deposition rate was corrected according to the difference between the measured thickness and 4000 nm. After that, a 100 nm thickness Pd-Cu-Si thin film was fabricated by using the corrected total deposition rate. The thicknesses of thin films were measured with a surface profiler (Dektak^3 ST, Veeco Instruments Inc.). The 100 nm thickness thin films were used for the measurement of the H_2 response and the 4000 nm thickness ones were used for the measurement of hydrogen induced LEC and the characterization of the films.

2.2 Measurement of the H_2 response

The H_2 response was observed by measuring the electric resistance changes of the thin films exposed in N_2 and H_2 under the atmospheric pressure. A thin film sample with a glass substrate was placed in a stainless chamber set up in an electric oven and then, its electric resistance was measured by 4-probes method using Au plated brass electrodes while the thin film sample was exposed in N_2 and H_2 alternately. The experimental temperature was controlled at 303 K. The H_2 response is expressed as the normalized value (R/R_0), where R and R_0 are the electric resistance of the thin film exposed in 100% H_2 and 100% N_2, respectively. The detail of the H_2 response measurement was explained in the previous report.[17)]

2.3 Measurement of the hydrogen induced linear expansion coefficient

The hydrogen induced linear expansion coefficients (LECs) of thin films were measured with a thermo mechanical analyzer (TMA, TMA4030SA, Bruker AXS K.K.) by tensile loading method. The sample for the measurement was a 4000 nm thickness, 10 mm length and 5 mm width thin film which was peeled off from a glass substrate and cut into the size. The load in tension was 0.5 g. Operating temperature was 298 K. To begin with, the sample was exposed in N_2. After that, the atmosphere gas was changed to H_2 and the longitudinal expansion of the sample was measured. The hydrogen induced LEC was calculated by the following equation.

$$\mathrm{LEC}\ (\%) = (L_{H_2} - L_0)/L_0 \times 100$$

L_{H_2}: length of the sample exposed in 100% H_2
L_0: initial length of the sample (= 10 mm)
The longitudinal expansion of the sample is expressed as $(L_{H_2} - L_0)$.

2.4 Alloy film characterization

The compositions of thin films were analyzed by inductively coupled plasma-atomic emission spectrometry (ICP-AES). The amorphous nature of the alloy was determined with an X-ray diffractometer (XRD, Ultima, Rigaku Corporation) using MoKα radiation. The initial crystals of heated thin films were determined with an XRD (RINT RAPID, Rigaku Corporation) using CuKα radiation. The crystallization temperatures of the alloys were measured with a differential scanning calorimeter (DSC, DSC6220, SII Nano-Technology Inc.). Ar gas was used for the atmosphere gas and the heating rate was 0.67 K/s. The microstructures of the thin films were observed with a transmission electron microscope (TEM, JEM-2100F, JEOL Ltd.).

3. Results and Discussion

3.1 H_2 response

Figure 2 shows the summarized composition map of the thin films indicating the 100% H_2 response measured at 303 K. The H_2 responses are classified into 7 data ranges expressed by different symbols. Samples (a) to (e) are the thin films used for the examination in following figures and their compositions are as follows: (a) $Pd_{80.7}Cu_{6.9}Si_{12.4}$, (b) $Pd_{77.5}Cu_{10.7}Si_{11.8}$, (c) $Pd_{75.3}Cu_{10.3}Si_{14.4}$, (d) $Pd_{78.9}Cu_{7.9}Si_{13.2}$ and (e) $Pd_{75.1}Cu_{12.3}Si_{12.6}$.

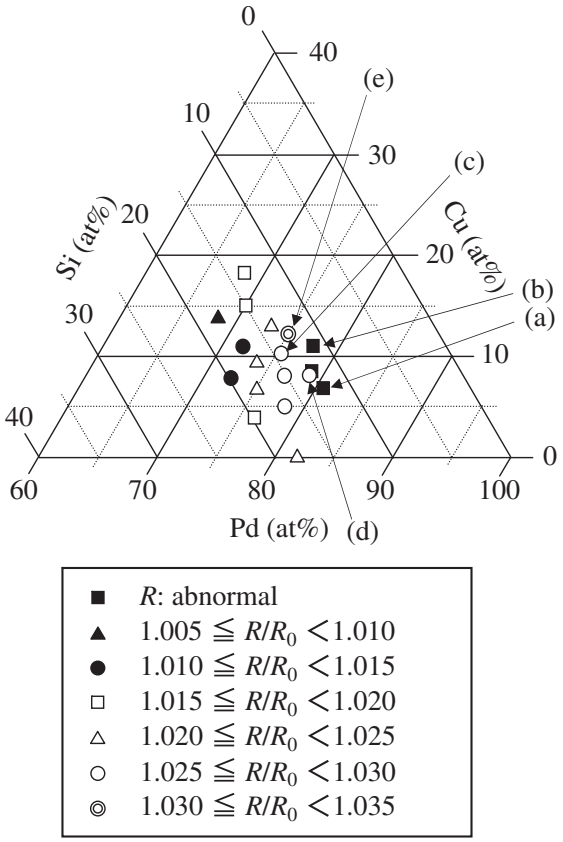

Fig. 2 Composition map of Pd-Cu-Si thin films indicating 100% H_2 response measured at 303 K. (a) $Pd_{80.7}Cu_{6.9}Si_{12.4}$, (b) $Pd_{77.5}Cu_{10.7}Si_{11.8}$, (c) $Pd_{75.3}Cu_{10.3}Si_{14.4}$, (d) $Pd_{78.9}Cu_{7.9}Si_{13.2}$, (e) $Pd_{75.1}Cu_{12.3}Si_{12.6}$ R/R_0: 100% H_2 response R: electric resistance of a sample in 100% H_2 R_0: electric resistance of a sample in 100% N_2.

Abnormal H_2 response transients were observed in several thin films (represented with filled square in Fig. 2). Figures 3(A) and (B) show the abnormal H_2 response transients observed in samples (a) and (b), respectively. On the other hand, Fig. 3(C) shows the normal H_2 response transient observed in sample (c). First of all, the thin films were exposed in 100% N_2 then, they were exposed in 100% H_2 and 100% N_2 alternately at intervals of 60 s. Sample (c) indicated a rapid increase in electric resistance induced by hydrogen absorption of Pd in the alloy, when the atmosphere gas was changed from N_2 to H_2. And then, the electric resistance took constant value as the solubility of hydrogen atoms into Pd reached its maximum limit. When the atmosphere gas was changed from H_2 to N_2, hydrogen atoms were desorbed from Pd, and the electric resistance decreased to the initial value indicated in N_2 atmosphere. This is a typical transient of a normal H_2 response of Pd-Cu-Si amorphous alloys.[17,18)]

On the other hand, samples (a) and (b) indicated different H_2 response transients from this as shown in Figs. 3(A) and (B). When the atmosphere gas was changed from N_2 to H_2, a rapid temporal decrease and a following steep increase in electric resistance were observed. After that, the electric resistance became stable in H_2. When the atmosphere gas

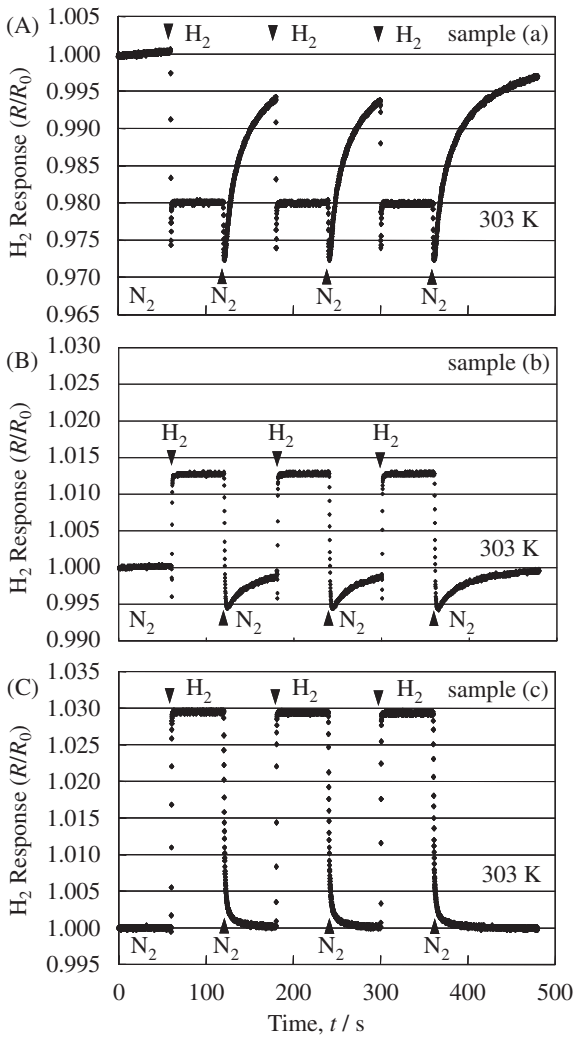

Fig. 3 Response transients of (A) (a) $Pd_{80.7}Cu_{6.9}Si_{12.4}$, (B) (b) $Pd_{77.5}Cu_{10.7}Si_{11.8}$ and (C) (c) $Pd_{75.3}Cu_{10.3}Si_{14.4}$ to 100% H_2 at 303 K. Gas-changing interval was 60 s.

was changed from H_2 to N_2, the electric resistance decreased temporarily and then, it turned to increases. The increasing speed was so slow that the electric resistance did not return to the initial value in N_2 within 60 s of gas-changing interval time.

In order to explain these abnormal H_2 response transients, we considered effects of the compositions of Pd-Cu-Si alloys on their microstructures. Samples (a) and (b) which indicated the abnormal H_2 response transients have higher Pd contents and lower Si contents than sample (c) with the normal one. Pd/Si atomic ratios of samples (a), (b) and (c) are 6.51, 6.57 and 5.23, respectively.

In our previous report,[18] we supposed that the number densities of trigonal prisms in Pd-Cu-Si metallic glassy alloys increased with increasing Si content (i.e. decreasing Pd/Si ratio). The trigonal prism is reported to be a structural unit of Pd-based amorphous alloys, and two types of the structures are suggested. One is a trigonal prism (6 Pd atoms around a Si atom) and the other is a trigonal prism capped with three half-octahedra (9 Pd atoms around a Si atom).[19]

Hirotsu *et al.*[20] have confirmed the existence of micro-crystalline domains with face-centered-cubic (fcc) Pd in the

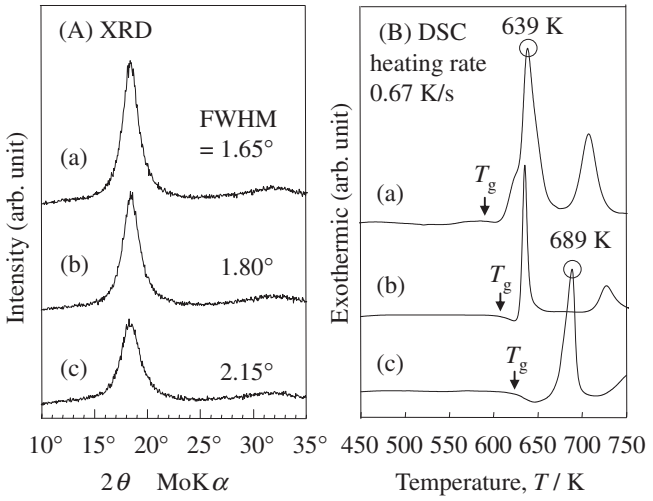

Fig. 4 (A) XRD and (B) DSC charts of (a) $Pd_{80.7}Cu_{6.9}Si_{12.4}$, (b) $Pd_{77.5}Cu_{10.7}Si_{11.8}$ and (c) $Pd_{75.3}Cu_{10.3}Si_{14.4}$. FWHM: Full Width of Half Maximum intensity T_g: glass transition temperature.

$Pd_{77.5}Cu_6Si_{16.5}$ alloy by high resolution electron microscopy (HREM). The average size of the domains was observed to vary from about 3.2 to 1.7 nm. By taking these studies into consideration, we can suppose samples (a) and (b) with high Pd/Si ratios have many Pd atoms which are unrelated to the formation of trigonal prisms and have structures including Pd-nanocrystals.

Figure 4(A) shows the summarized plots of XRD patterns of samples (a), (b) and (c) indicating the full width of half maximum intensity (FWHM) of each main peak. The fact that FWHMs of samples (a) and (b) are narrower than that of sample (c) suggests that the crystallinities of sample (a) and (b) are higher than that of sample (c). Figure 4(B) shows DSC curves of them. Samples (a) and (b) indicate the first exothermic peaks corresponding to crystallization at around 639 K, while sample (c) indicates it at not around 639 K but 689 K. From Fig. 4(B), it can be expected that the initial crystals of the two sample groups (the group of samples (a) and (b) and the group of sample (c)) are different.

In order to confirm this expectation, we heated samples (a) and (c) to the corresponding peak-temperatures, (a) 639 K and (c) 689 K, at which exothermic peaks were indicated by DSC measurement, for making initial crystals of these samples to grow. A differential scanning calorimeter (DSC) was used to heat the thin films with heating rate of 0.67 K/s in Ar gas atmosphere. The initial crystals of these samples were determined with an XRD using CuKα radiation. The XRD charts are shown in Fig. 5. The initial crystals of sample (a) were determined to be Pd and $PdSi_5$. And that of sample (c) was determined to be Pd_3Si which is thought to be a constituent unit of a trigonal prism. From these results, it can be stated that sample (a) has many Pd-nanocrystals in its structure. In contrast, sample (c) has less Pd-nanocrystals than sample (a), and trigonal prisms are primary structural unit of this sample.

The microstructures and the electron diffraction patterns of as-deposited samples (a) and (c) were observed with a TEM. Figures 6(A) and (B) show the high resolution transmission electron microscopy (HRTEM) image and the electron

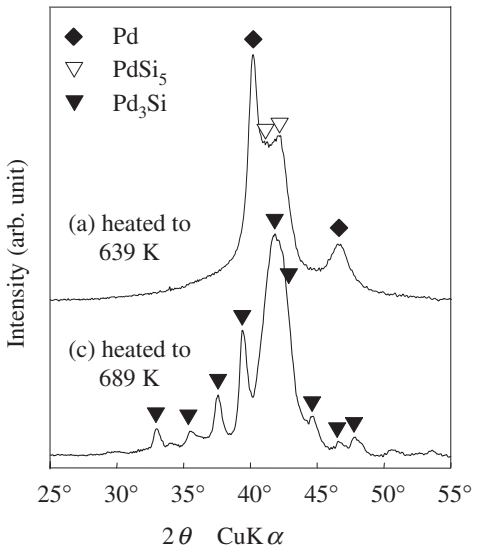

Fig. 5 XRD charts of (a) $Pd_{80.7}Cu_{6.9}Si_{12.4}$ heated to 639 K and (c) $Pd_{75.3}Cu_{10.3}Si_{14.4}$ heated to 689 K. Heating rate was 0.67 K/s.

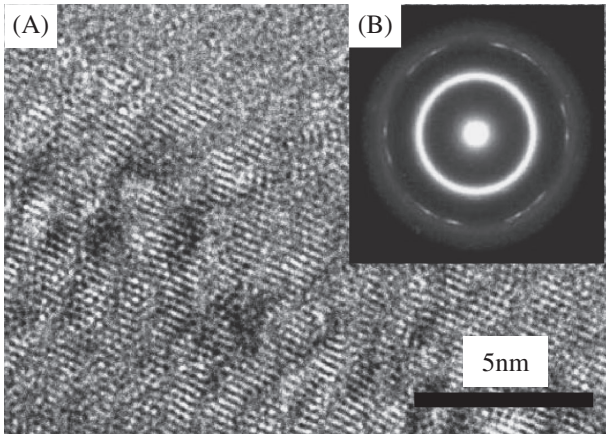

Fig. 6 (A) HRTEM image and (B) electron diffraction pattern of (a) $Pd_{80.7}Cu_{6.9}Si_{12.4}$.

diffraction pattern of sample (a), respectively. Many grains with lattice fringes can be observed, and their diameters are estimated to be about 2 nm. Diffraction spots on the diffraction ring corresponding to a spacing of 0.14 nm, which is corresponding to the spacing of (220) of fcc-Pd, can be observed in Fig. 6(B). The other possible diffraction spots, e.g. (111) and (200), are probably hidden among the halo pattern of the amorphous phase. On the other hand, the HRTEM image of sample (c) shows no grains with lattice fringes in Fig. 7(A), and the diffraction pattern of it shows no spots on the diffraction ring in Fig. 7(B). From these results, it can be confirmed that sample (a) has many Pd-nanocrystals in its amorphous matrix, while sample (c) does not have them.

The mechanism of the abnormal H_2 response transient was discussed by considering the existence of Pd-nanocrystals in the structure. Figure 8 shows the schematic illustrations of the possible mechanism for the abnormal H_2 response transient observed in sample (a).

In the state of Fig. 8(1), the sample (a) is exposed in N_2 and indicates constant electric resistance. Pd-nanocrystals do not form electrical contacts with each other in this state. Randomly distributed atoms (Pd, Cu and Si), Pd-clusters, trigonal prisms and free volume[21] are possibly present as an amorphous matrix among the Pd-nanocrystals; trigonal prisms and free volume are not drawn in Fig. 8. The amorphous matrix has higher electric resistance than Pd-nanocrystals,[22] because of its disorder scattering.[23]

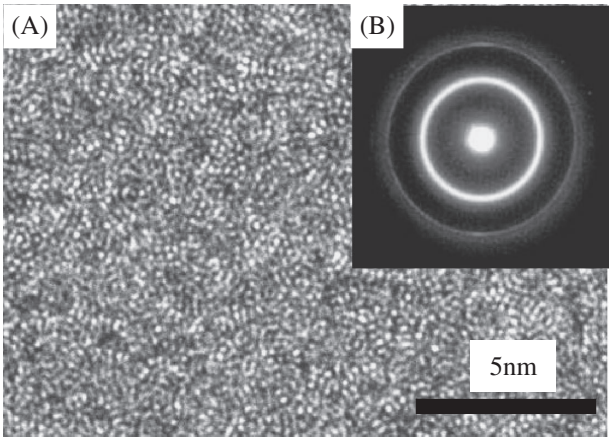

Fig. 7 (A) HRTEM image and (B) electron diffraction pattern of (c) $Pd_{75.3}Cu_{10.3}Si_{14.4}$.

In the state of Fig. 8(2), the atmosphere gas is changed from N_2 to H_2 and then, a rapid temporal decrease in electric resistance is observed. Hydrogen molecules are dissociated into hydrogen atoms at the surface of a Pd-Cu-Si thin film and then, the hydrogen atoms transfer along the pathways of the amorphous matrix among Pd-nanocrystals. We think that the transfer speed of hydrogen atoms through the amorphous matrix is faster than that through the inside of Pd-nanocrystals. Because Pd-clusters existing in the amorphous matrix are much smaller than Pd-nanocrystals, therefore the diffusion distance of hydrogen atoms into Pd-clusters is much shorter than that into Pd-nanocrystals. That is, the time required for hydrogen to diffuse into a Pd-cluster until its maximum solubility is shorter than the time for it to diffuse into a Pd-nanocrystal.

With regard to the transfer speeds of hydrogen atoms through an amorphous matrix and a crystal, Lee and Stevenson[24] have studied the diffusion coefficients of hydrogen in amorphous and crystalline Pd-Si alloys at 292 K. According to their study, the diffusion coefficient of hydrogen in amorphous state strongly depends on hydrogen concentration and takes higher values than that in crystalline state at high hydrogen concentrations (e.g. $H/Pd > 10^{-3}$ for $Pd_{83}Si_{17}$). The hydrogen concentrations (H/Pd) of $Pd_{83}Si_{17}$ in amorphous and crystalline states are 0.044 and 0.016, respectively at room temperature and hydrogen pressure of 1 atom. Therefore, the diffusion coefficient of hydrogen in an amorphous matrix is larger than that in a crystal under the H_2 response measurement condition in this study: 100% H_2 under the atmospheric pressure (hydrogen pressure of 100 kPa) at 303 K. They explained the higher hydrogen solubility and strong dependence of the diffusion coefficient on hydrogen concentration in amorphous state by a broad range of energy states for the hydrogen incorporation in the amorphous state.

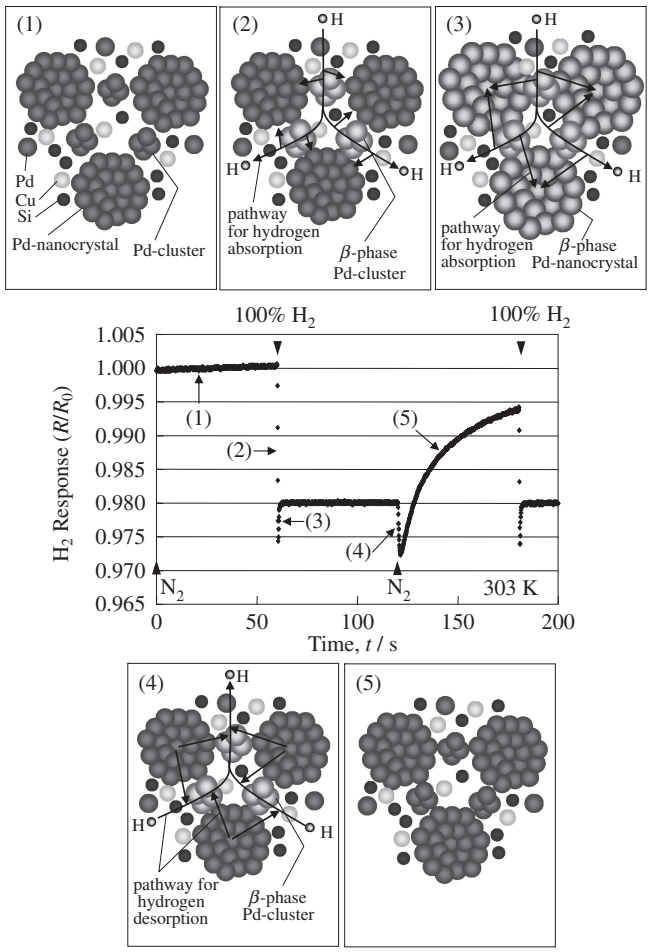

Fig. 8 Schematic illustrations of the possible mechanism of the abnormal H_2 response transient observed in (a) $Pd_{80.7}Cu_{6.9}Si_{12.4}$ at 303 K. (1) Pd-nanocrystals do not form electrical contacts with each other in N_2 atmosphere. (2) Hydrogen atoms transfer along the pathways of the amorphous matrix among Pd-nanocrystals. Pd-clusters in the amorphous matrix absorb hydrogen atoms, and transfer to β-phase Pd with expanding their volume and increasing their electric resistance. This volume expanded Pd-clusters connect the separately located Pd-nanocrystals and form the electrical contacts of the Pd-nanocrystals to decrease the electric resistance of the thin film. The change in the H_2 response is derived from the sum of the electric resistance of these conflicting behaviors. (3) Hydrogen atoms diffuse into Pd-nanocrystals. Pd-nanocrystals transfer to β-phase Pd with expanding their volume and increasing their electric resistance. The observed increase in the electric resistance is due to the change in electric resistance of Pd-nanocrystals. (4) Hydrogen atoms are desorbed from β-phase Pd, and transfer along the pathways of the amorphous matrix. The electric resistance decreases by the desorption of hydrogen from β-phase Pd-nanocrystals. (5) Pd-nanocrystals gradually lose the electrical contacts with each other, which is caused by volume shrinkage of Pd-clusters with desorbing hydrogen atoms.

Pd-clusters in the amorphous matrix absorb hydrogen atoms and transfer to β-phase Pd, a hydride of Pd, with expanding their volume. This volume expanded Pd-clusters connect the separately located Pd-nanocrystals and form the electrical contacts of the Pd-nanocrystals, which causes a decrease in the electric resistance of a thin film. Pd transfers to β-phase Pd by absorbing hydrogen[25] under the H_2 response measurement condition in this study. The lattice constants of fcc-Pd and β-phase Pd are 0.3890 nm and 0.4025 nm, respectively.[6] The linear expansion coefficient (LEC) and volume expansion coefficient (VEC) of Pd exposed in 100% H_2 under the atmospheric pressure at 303 K are estimated to be 3.47% and 10.78%, respectively by using these lattice constants. However at the same time, the electric resistance of the Pd-clusters in the amorphous matrix increase due to hydrogen absorption. This is the conflicting behavior of electric resistance with a decrease by the formation of electrical contacts of Pd-nanocrystals. And the change in the H_2 response is derived from the sum of the electric resistance of these conflicting behaviors. In sample (a), the degree of a decrease in electric resistance by the electrical contacts of Pd-nanocrystals is much larger than that of an increase by hydrogen absorption of Pd-clusters.

In the state of Fig. 8(3), the electric resistance is changed to an increase and then, takes constant value. In this state, hydrogen atoms diffuse into Pd-nanocrystals. Pd-nanocrystals transfer to β-phase Pd with expanding their volume and increasing their electric resistance.

These conflicting behaviors of the electric resistance of the thin film in the states of Figs. 8(2) and (3) are caused by hydrogen absorption of Pd. Therefore, volume expansion of Pd (Pd-nanocrystals and Pd-clusters) and an increase in the electric resistance of Pd are thought to proceed at the same time. But in the H_2 response transient, a rapid temporal decrease in electric resistance is observed at first and then, a steep increase and stabilization are observed when the atmosphere gas is changed from N_2 to H_2. Observed time lags between the two conflicting behaviors of electric resistance can be explained by the different transfer speeds of hydrogen atoms relating to two kinds of pathways, inside of Pd-nanocrystals and the amorphous matrix, along which hydrogen atoms transfer in the structure of the thin film, as shown in Figs. 8(2) and (3).

The difference of the degree of temporary decreases in electric resistance between samples (a) and (b), shown in Figs. 3(A) and (B), is possibly related to the number density of Pd-nanocrystals. The degree will become larger with an increase in it. The number density of Pd-nanocrystals of sample (a) is probably larger than that of sample (b), because FWHM of sample (a) is narrower than that of sample (b), as shown in Fig. 4(A).

In the state of Fig. 8(4), the atmosphere gas is changed from H_2 to N_2, and the hydrogen atoms are desorbed from β-phase Pd, leading to a decrease in electric resistance. As with hydrogen absorbing process in Fig. 8(2), desorbed hydrogen atoms transfer along the pathways of the amorphous matrix. Therefore, hydrogen desorption from Pd-clusters in the amorphous matrix will occur after that from Pd-nanocrystals. In this state, the electrical contacts of Pd-nanocrystals are still formed due to the delay of hydrogen desorption from the Pd-clusters.

In the state of Fig. 8(5), the electric resistance gradually increases with the electrical contacts of Pd-nanocrystals open, which is caused by volume shrinkage of Pd-clusters with desorbing hydrogen atoms. The time required for opening the electrical contacts completely is much longer than that for forming the contacts.

3.2 Hydrogen induced linear expansion coefficient

100% H_2 induced LEC at 298 K is plotted against Pd/Si atomic ratio in Fig. 9. The codes (a) to (e) are corresponding

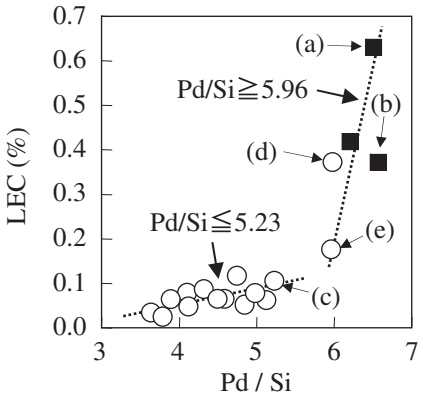

Fig. 9 Correlation between 100% H_2 induced linear expansion coefficient (LEC) at 298 K and Pd/Si atomic ratio. Filled squares represent the samples that showed the abnormal H_2 response transients. The codes (a) to (e) are corresponding to the samples shown in Fig. 2. Broken lines are regression lines for the Pd/Si $\leqq$ 5.23 group and the Pd/Si $\geqq$ 5.96 group.

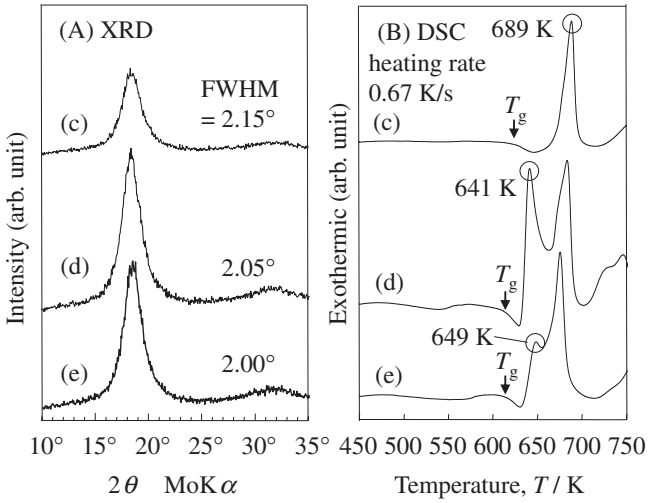

Fig. 10 (A) XRD and (B) DSC charts of (c) $Pd_{75.3}Cu_{10.3}Si_{14.4}$, (d) $Pd_{78.9}Cu_{7.9}Si_{13.2}$ and (e) $Pd_{75.1}Cu_{12.3}Si_{12.6}$.

to the samples shown in Fig. 2, and the filled squares represent the samples that showed the abnormal H_2 response transients. All of the data can be classified into two groups, Pd/Si $\leqq$ 5.23 and Pd/Si $\geqq$ 5.96, with different positive slopes of regression lines indicated by broken lines. The slope of the Pd/Si $\geqq$ 5.96 group is much steeper than that of the Pd/Si $\leqq$ 5.23 group. As we mentioned above, Pd expands its volume by transferring to β-phase Pd. Pd is a primary element that absorbs hydrogen in a Pd-Cu-Si alloy, therefore LEC should show a positive correlation with Pd content. And also, LEC shows a positive correlation with the amount of absorbed hydrogen.[7)]

In order to trace the origin of the different slopes between two sample groups in Fig. 9, FWHMs of XRD peaks and the crystallization temperatures of samples (c), (d) and (e) were examined. Figure 10(A) shows XRD patterns of them indicating FWHM of each main peak. FWHMs of samples (d) and (e) are narrower than that of sample (c). This result suggests that the crystallinities of samples (d) and (e) are higher than that of sample (c). Figure 10(B) shows DSC curves of them. Samples (d) and (e) indicate the first exothermic peaks corresponding to crystallization at 641 K and 649 K, respectively, while sample (c) indicates the peak at 689 K. From these results and the relating results in Fig. 4(B) and Fig. 5, the existence of Pd-nanocrystals are expected in samples (d) and (e), while a trigonal prism is thought to be a primary structural unit of sample (c). Therefore, the much steeper slope of the Pd/Si $\geqq$ 5.96 group is due to the existence of Pd-nanocrystals in the structures. Additionally, it can be supposed that Pd-nanocrystals absorb much more hydrogen atoms than Pd in an amorphous matrix: Pd-clusters, randomly distributed Pd atoms and Pd atoms forming trigonal prisms. The difference of hydrogen absorbing ability between them results in the significant difference of the slopes of regression lines in Fig. 9.

Figure 11 shows the correlation between the 100% H_2 response at 303 K and 100% H_2 induced LEC at 298 K. In this figure, the data of the samples indicated the abnormal H_2 response transients are not plotted. As with Fig. 9, all of the data can be classified into two groups, Pd/Si $\leqq$ 5.23 and

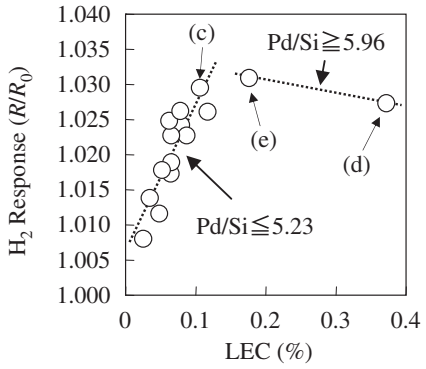

Fig. 11 Correlation between 100% H_2 response at 303 K and 100% H_2 induced linear expansion coefficient (LEC) at 298 K. The codes (c) to (e) are corresponding to the samples shown in Fig. 2. Broken lines are regression lines for the Pd/Si $\leqq$ 5.23 group and the Pd/Si $\geqq$ 5.96 group.

Pd/Si $\geqq$ 5.96, with different slopes of regression lines indicated by broken lines. The data whose LEC are within 0.12% indicate a positive correlation between the H_2 response and LEC, and they are corresponding to the Pd/Si $\leqq$ 5.23 group in Fig. 9. In contrast, the data whose LEC are over 0.18%, samples (d) and (e), indicate a weak negative correlation, and they are corresponding to the Pd/Si $\geqq$ 5.96 group in Fig. 9.

There is a positive correlation between the H_2 response and the amount of absorbed hydrogen.[4)] And also, the volume expansion coefficient is proportional to the amount of absorbed hydrogen.[7)] Therefore, the H_2 response and LEC should show a positive correlation, and the proportional slope of the regression line corresponding to the Pd/Si $\leqq$ 5.23 group is according to this theory.

The reason of the lower H_2 response of the Pd/Si $\geqq$ 5.96 group than that expected with extrapolating from the regression line of the Pd/Si $\leqq$ 5.23 group can be explained by the mechanism discussed in Fig. 8. This result suggests that large parts of the absorbed hydrogen of the Pd/Si $\geqq$ 5.96 group probably make less contribution to the H_2 response. The samples in the Pd/Si $\geqq$ 5.96 group have Pd-nanocrystals

in their structure, and the Pd-nanocrystals form electrical contacts with each other by hydrogen absorption, as with sample (a). The H_2 response of the group is derived from the sum of the electric resistance induced by two conflicting behaviors: an increase in electric resistance of Pd by absorbing hydrogen and a decrease by the formation of electrical contacts of Pd-nanocrystals. Therefore, the H_2 response of the Pd/Si $\geqq$ 5.96 group indicated lower value than that expected from their high LEC. Samples (d) and (e) had Pd-nanocrystals as well as samples (a) and (b), but samples (d) and (e) indicated the normal H_2 response although samples (a) and (b) indicated the abnormal H_2 response. The reason of this can be possibly explained by the difference of the number densities of Pd-nanocrystals in the samples. Pd/Si atomic ratios of samples (d) and (e) are lower than those of samples (a) and (b), and FWHMs of XRD peaks of samples (d) and (e) are wider than those of samples (a) and (b). These results suggest that the number densities of Pd-nanocrystals of samples (d) and (e) are smaller than those of samples (a) and (b). Therefore, the effect of forming electrical contacts of Pd-nanocrystals on the H_2 responses was so small in samples (d) and (e), that the abnormal H_2 response transients were not observed as actual measurement data.

4. Summary

In this study, thin films of Pd-Cu-Si metallic glassy alloys with varying composition were prepared by simultaneous three sources sputtering method using a rotating mechanism of substrates. Their H_2 responses and the hydrogen induced LEC were measured. The obtained results in this study are summarized as follows.

(1) Several thin films indicated abnormal H_2 response transients consisting of complex behaviors, an increase and a decrease, in electric resistance when the thin films were exposed in H_2. These thin films have higher Pd/Si atomic ratios than those indicated normal H_2 response transients. Additionally, by the characterization of the thin films, the existence of Pd-nanocrystals of about 2 nm in diameter was observed in the amorphous matrix which possibly includes Pd-clusters as well as Pd atoms.

The mechanism of the abnormal H_2 response transient can be explained by two conflicting behaviors in electric resistance of the thin films when they are exposed in H_2: a decrease by the formation of electrical contacts of Pd-nanocrystals connected with volume expanded Pd-clusters by hydrogen absorption, and a following increase by hydrogenation of Pd-nanocrystals.

Observed time lags between the two conflicting behaviors in electric resistance can be explained by the different transfer speeds of hydrogen relating to two kinds of pathways, inside of Pd-nanocrystals and the amorphous matrix, along which hydrogen atoms transfer in the structure. The transfer speed of hydrogen atoms through the amorphous matrix is thought to be faster than that through the inside of Pd-nanocrystals.

(2) The Pd-nanocrystals significantly affected on LEC and the H_2 response. The thin films with them indicated much higher LEC than the thin films without them. However, the thin films with them did not indicate the high H_2 response expected from their high LEC.

Possible explanations of these results are as follows. Pd-nanocrystals can possibly absorb much more hydrogen atoms than Pd in an amorphous matrix, consisting of Pd-clusters, randomly distributed Pd atoms and Pd atoms forming trigonal prisms, resulting in the high LEC.

In contrast, Pd-nanocrystals form electrical contacts with each other resulting in a decrease in electric resistance of a thin film as well as increasing their electric resistance with absorbing hydrogen. Therefore, the H_2 responses of the thin films with Pd-nanocrystals took lower values than the expected values, because the H_2 responses are derived from the sum of the electric resistance induced by the two conflicting behaviors.

Pd is a primary element that absorbs hydrogen in a Pd-Cu-Si metallic glassy alloy. Therefore, the composition with high Pd content is desirable for the large H_2 response of a hydrogen sensor. However, excess Pd content (Pd/Si $\geqq$ 5.96 in this study) causes a composite structure of Pd-nanocrystals and an amorphous matrix, resulting in the abnormal H_2 response transient or the low H_2 response for its high LEC.

REFERENCES

1) U.S. Department of Energy: Fuel Cells, Technical Plan, Multi-Year Research, Development and Demonstration Plan, (2007).
2) H. S. Chen and D. Turnbull: Acta Metall. **17** (1969) 1021–1031.
3) F. A. Lewis: *The Palladium Hydrogen System*, (Academic Press, London, 1967) p. 11.
4) F. A. Lewis: *The Palladium Hydrogen System*, (Academic Press, London, 1967) p. 52.
5) K. Baba and Y. Sakamoto: Mater. Sci. Eng. **99** (1988) 539–542.
6) E. Wicke and H. Brodowsky: *Hydrogen in Metals II*, (Springer-Verlag, Berlin, 1978) p. 77.
7) K. Salama and C. R. Ko: J. Appl. Phys. **51** (1980) 6202–6209.
8) A. Inoue: Acta Mater. **48** (2000) 279–306.
9) K. Aoki, M. Kamachi and T. Masumoto: J. Non-Cryst. Solids **62** (1984) 679.
10) S. Hata, K. Sato and A. Shimokohbe: Proc. SPIE, MICRO/MEMS'99 **3892** (1999) 97–108.
11) S. Nakano, S. Yamaura, K. Yubuta, H. Kimura and A. Inoue: J. Mater. Sci. Soc. Jpn. **44** (2006) 203–208.
12) Y. Liu, S. Hata, K. Wada and A. Shimokohbe: Jpn. J. Appl. Phys. **40** (2001) 5382–5388.
13) R. Yamauchi, S. Hata, J. Sakurai and A. Shimokohbe: Jpn. J. Appl. Phys. **45** (2006) 5911–5919.
14) J. Sakurai, S. Hata and A. Shimokohbe: Jpn. J. Appl. Phys. **48** (2009) 025503-1.
15) H. S. Chen and D. Turnbull: Acta Metall. **17** (1969) 1021.
16) H. S. Chen and B. K. Park: Acta Metall. **17** (1973) 395.
17) S. Kajita, S. Yamaura, H. Kimura, K. Yubuta and A. Inoue: IEE Trans. SM **128** (2008) 225–229.
18) S. Kajita, S. Yamaura, H. Kimura and A. Inoue: Mater. Trans. **51** (2010) 2133–2138.
19) T. Fukunaga and K. Suzuki: Sci. Rep. Inst. Tohoku Univ. **A29** (1981) 153–175.
20) Y. Hirotsu, M. Uehara and M. Ueno: J. Appl. Phys. **59** (1986) 3081–3086.
21) M. H. Cohen and D. Turnbull: J. Chem. Phys. **31** (1959) 1164–1169.
22) P. Duwez, R. H. Willens and R. C. Crewdson: J. Appl. Phys. **36** (1965) 2267–2269.
23) K. V. Rao: *Amorphous Metallic Alloys*, (Butterworths, London, 1983) p. 402.
24) Y. S. Lee and D. A. Stevenson: J. Non-Cryst. Solid. **72** (1985) 249–266.
25) E. Wicke and H. Brodowsky: *Hydrogen in Metals II*, (Springer-Verlag, Berlin, 1978) p. 81.